

Communication

# Alkene Epoxidations Mediated by Mn-Salen Macrocyclic Catalysts

Andrea Pappalardo<sup>1,2</sup>, Francesco P. Ballistreri<sup>1</sup>, Rosa Maria Toscano<sup>1</sup>, Maria Assunta Chiacchio<sup>3</sup>, Laura Legnani<sup>3</sup>, Giovanni Grazioso<sup>4</sup> , Lucia Veltri<sup>5</sup> and Giuseppe Trusso Sfrazzetto<sup>1,2,\*</sup> 

- <sup>1</sup> Department of Chemical Sciences, University of Catania, 95125 Catania, Italy; andrea.pappalardo@unict.it (A.P.); fballistreri@unict.it (F.P.B.); rmtoscano@unict.it (R.M.T.)
- <sup>2</sup> Research Unit of Catania, National Interuniversity Consortium for Materials Science and Technology (I.N.S.T.M.), 95125 Catania, Italy
- <sup>3</sup> Department of Drug Sciences, University of Catania, Viale A. Doria 6, 95125 Catania, Italy; ma.chiacchio@unict.it (M.A.C.); laura.legnani@unipv.it (L.L.)
- <sup>4</sup> Dipartimento di Scienze Farmaceutiche, Università degli Studi di Milano, Via L. Mangiagalli 25, 20133 Milan, Italy; giovanni.grazioso@unimi.it
- <sup>5</sup> Laboratory of Industrial and Synthetic Organic Chemistry (LISOC), Department of Chemistry and Chemical Technologies, University of Calabria, Via P. Bucci 12/C, 87036 Arcavacata di Rende, Italy; lucia.veltri@unical.it
- \* Correspondence: giuseppe.trusso@unict.it; Tel.: +39-095-7385201

**Abstract:** Three new chiral Mn macrocycle catalysts containing 20 or 40 atoms in the macrocycle were synthesized and tested in the enantioselective epoxidation of cis- $\beta$ -ethyl-styrene and 1,2-dihydronathalene. The effect of the presence of a binaphthol (BINOL) compound in the catalyst backbone has been evaluated, including by Density Functional Theory (DFT) calculations.

**Keywords:** enantioselective; epoxidation; Mn catalyst; alkene; DFT



**Citation:** Pappalardo, A.; Ballistreri, F.P.; Toscano, R.M.; Chiacchio, M.A.; Legnani, L.; Grazioso, G.; Veltri, L.; Trusso Sfrazzetto, G. Alkene Epoxidations Mediated by Mn-Salen Macrocyclic Catalysts. *Catalysts* **2021**, *11*, 465. <https://doi.org/10.3390/catal11040465>

Academic Editor:  
Jean-Marc Campagne

Received: 17 March 2021  
Accepted: 31 March 2021  
Published: 2 April 2021

**Publisher's Note:** MDPI stays neutral with regard to jurisdictional claims in published maps and institutional affiliations.



**Copyright:** © 2021 by the authors. Licensee MDPI, Basel, Switzerland. This article is an open access article distributed under the terms and conditions of the Creative Commons Attribution (CC BY) license (<https://creativecommons.org/licenses/by/4.0/>).

## 1. Introduction

Asymmetric epoxidation of unfunctionalized prochiral olefins catalyzed by chiral (salen)Mn(III) complexes has proven to be one of the most useful reactions in organic synthesis since it generates chiral epoxides containing two new stereocenters, which can be easily transformed into a large variety of compounds useful in industrial, biological, pharmaceutical and agricultural fields [1]. The origins of high enantioselectivity in this reaction have been extensively studied [2] but, until now, not fully elucidated. A possible electronic effect of the 5,5'-substituents in the salen ligand is invoked [3,4], but the most common explanation is attributed to the directions of approach of the alkene to the manganese active site (manganese-oxo) [5]. The side-on approach where the double bond of the alkene is parallel to the salen ligand is generally accepted, but four main directions to the Mn-oxo [6,7] moiety have been proposed in the literature (Figure 1).

Katsuki et al. hypothesized that the substrate approaches the catalyst along the Mn–N bond (Figure 1, path A) [8–10]. In addition, Jacobsen assumed that (salen)Mn=O has a planar conformation and steric bulk at the 3,3'- and 5,5'-positions, thus forcing the substrate to approach over the ethylenediamine backbone (Figure 1, path B) [11–15]. Furthermore, Katsuki also proposed an approach direction by pathway C, along the 5,5'-position [16,17]. It is generally accepted that the increase of steric bulkiness in the 3,3'-positions of the salen ligand enhances enantioselectivity, suggesting that the alkene does not approach from this direction to the metal center (Figure 1, path D) [18–26].

More recently, a new justification about the origin of enantioselectivity was proposed by Corey et al. [14,15]. They asserted that none of these explanations seem to be plausible when the mechanism is represented in three dimensions. They proposed that the pre-transition state geometry could be stabilized by electrostatic interaction between a partial positive charge localized in the benzylic carbon atom of alkene and the partial negative

charge of phenoxy oxygen of the catalyst (Figure 2a). In this hypothesis, the transition state assembly is slightly similar to a [3 + 2] cycloaddition.

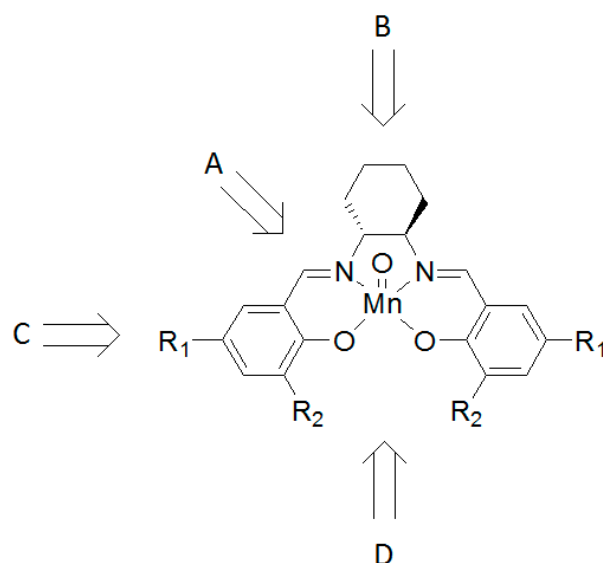


Figure 1. Proposed directions of approach to the active Mn-oxo moiety of (salen)Mn.

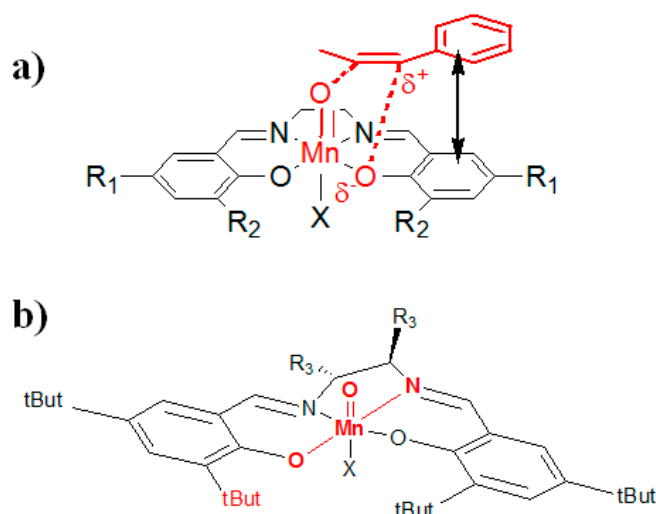


Figure 2. (a) Pre-transition state geometry invoked by Corey; (b) spatial arrangement of the salen catalyst.

A geometric consequence of the canted arrangement of the salen rings due to the configuration of the chiral diimine bridge is that the neighboring *t*-butyl groups in the ortho position to the coordinated phenolic oxygens occupy spaces on opposite faces of the N–Mn–O plane (Figure 2b). Considering Corey’s hypothesis, the orientation of substrates, in particular of aromatic conjugate alkenes, in the (salen)Mn-oxo complex avoids unfavorable steric repulsion with the *t*-butyl groups, taking advantage of stabilizing  $\pi$ -stacking of the aromatic ring of the alkene and the aryloxy group of the catalyst (Figure 2a).

## 2. Results and Discussion

To better understand the importance of the approach direction as well as the importance of bulkiness in the 3,3’-positions, we report here three new chiral Mn macrocycle catalysts based on the classic Jacobsen’s salen catalyst bearing an (*R*)-(+)-BINOL unit in the 3,3’-position of the salen backbone (see Chart 1). These catalysts differ in the size of

the macrocycle, having 20 members (in the case of Mn-M20) or 40 members (in the case of Mn-M40-DiPh and Mn-M40-Cycl) in the macrocycle. In addition, their activity towards epoxidation by using two alkene models (cis- $\beta$ -methyl-styrene and 1,2-dihydronaphthalene) was evaluated.

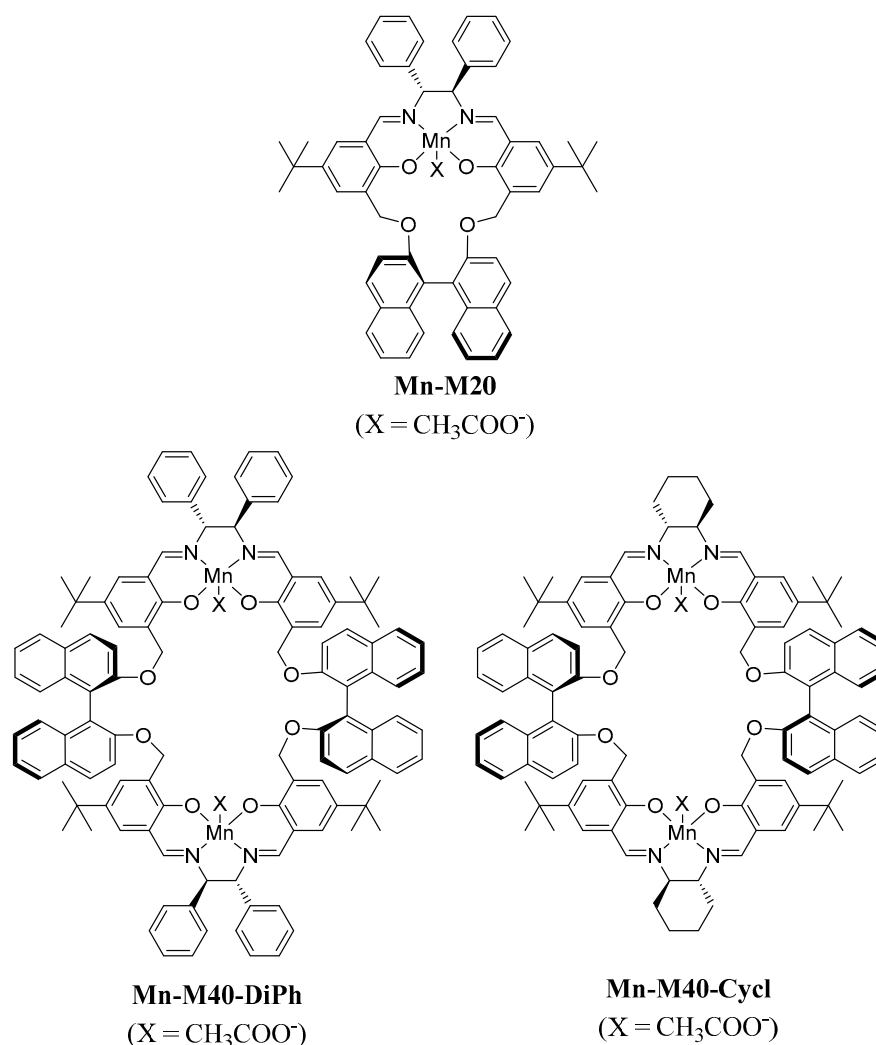


**Chart 1.** Chemical structures of Mn macrocycle catalysts.

Mn catalysts reported in Chart 1 were obtained starting from the corresponding macrocycle ligands (M20 and M40) [16,17] by complexation with manganese(III) acetate in ethanol [18]. Compounds were collected by filtration and characterized by ESI-MS (Electrospray Ionization-Mass Spectrometry) measurements. The chiral diimine bridge of Mn-M20 and Mn-M40-DiPh is (1*R*,2*R*)-diphenyl-ethyl group, while Mn-M40-Cycl leads a (1*R*-trans)-cyclohexyl group.

Table 1 shows epoxidation results in terms of conversions, epoxide yields and enantiomeric excess (EE). The results clearly show a different epoxidation rate based on the nature of the alkene: reactions with 1,2-dihydronaphthalene (Table 1, entries 7–12) are faster than reactions with cis- $\beta$ -methyl-styrene (Table 1, entries 1–6) [19–21]. Moreover, the presence of PPNO (4-phenyl-pyridine N-oxide) as a coligand increases reaction rates, conversions and enantiomeric excesses, suggesting a favorable electronic effect to the manganese metal center [22].

**Table 1.** Enantioselective epoxidation of alkenes with NaClO catalyzed by Mn macrocycle catalysts <sup>a</sup>.

Alkene	Entry	Catalyst	Time (min)	Conv. <sup>b</sup> (%)	Yield <sup>b</sup> (%)	EE <sup>b</sup> (%)
cis- $\beta$ -methyl-styrene	1 <sup>c</sup>	Mn-M20	300	80	88	16
	2	Mn-M20	240	90	88	27
	3 <sup>c</sup>	Mn-M40-DiPh	420	78	84	17
	4	Mn-M40-DiPh	300	87	82	31
	5 <sup>c</sup>	Mn-M40-Cycl	420	77	85	12
	6	Mn-M40-Cycl	300	89	84	30
1,2-dihydro-naphthalene	7 <sup>c</sup>	Mn-M20	60	92	93	23
	8	Mn-M20	30	95	94	38
	9 <sup>c</sup>	Mn-M40-DiPh	90	90	91	25
	10	Mn-M40-DiPh	30	88	89	35
	11 <sup>c</sup>	Mn-M40-Cycl	90	80	93	29
	12	Mn-M40-Cycl	30	90	99	36

<sup>a</sup> In all the experiments, alkene = 0.14 M, catalyst = 0.007 M, coligand = 4-PPNO = 0.07 M, NaClO = 0.14 M, Na<sub>2</sub>HPO<sub>4</sub> = 0.05 M, buffered at pH = 11.2. In all the cases, configuration of epoxides is determined by measuring the optical rotation. <sup>b</sup> Determined by GC on chiral columns. <sup>c</sup> No coligand added.

Although these macrocycle catalysts possess different chiral diimine bridges (diphenyl or cyclohexyl) and, consequently, different steric hindrances to the Mn-oxo group along approach directions A and B (reported in Figure 1), the enantiomeric excess values were similar. These data suggest that steric restrictions closer to the active catalyst site do not play a primary role in the determination of the enantioselectivity values. Furthermore, the different size of the macrocycles and the different steric hindrance along pathway D represented in Figure 1 did not lead to different EE values. The lower EE values obtained with these macrocycles with respect to other Mn-salen catalysts should have been due to the presence of the chiral (*R*)-(+)-BINOL compound that can reduce the efficiency of the enantioselective oxygen transfer.

#### Theoretical Calculations

In order to rationalize the enantiomeric excess results, DFT studies were performed on the simplest catalyst. First, our attention was focused on Mn-M20 that was optimized and the obtained 3D plots together with the corresponding activated forms containing the Mn=O species formed in the presence of NaClO are reported in Figure 3.

The catalyst and its activated form showed overlapping structures characterized by the steric hindrances of BINOL groups.

In order to rationalize the enantioselectivity of the reaction, the two transition states leading to the two possible enantiomeric epoxides were located by using DFT calculations [23–26]. The computational study was carried out on the epoxidation reaction involving Mn-M20 in its activated form as a catalyst and cis- $\beta$ -methyl-styrene, which seems to be a good compromise between the size of the system and the accuracy of the calculation.

The located transition state (TS) present the expected imaginary frequencies on the O transfer (see Supporting Information). In Figure 4, the formation bond distances are shown. The favored (2*S*,3*R*)-TS (Figure 4A) had the bond less formed (1.77 Å) than the (2*R*,3*S*)-TS (Figure 4B) (1.74 Å).

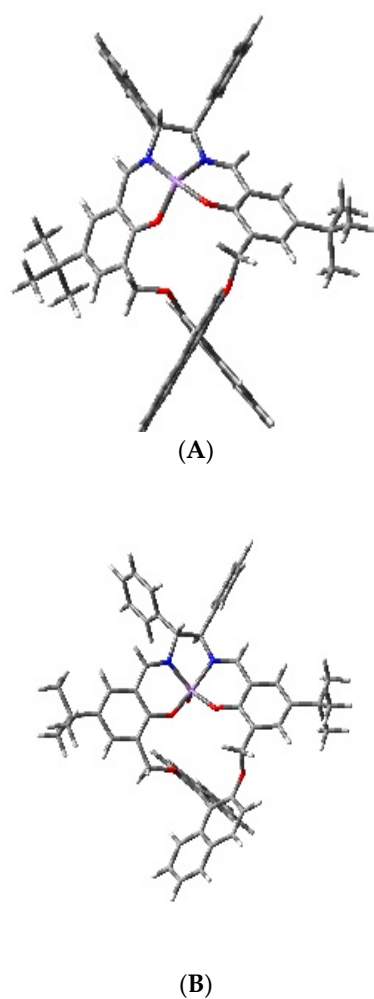


**Figure 3.** 3D-plots of Mn-M20 (A) and the corresponding activated structure (B) minimized at the b3lyp/def2svp level for Mn and b3lyp/6-31 g(d) for all other atoms.

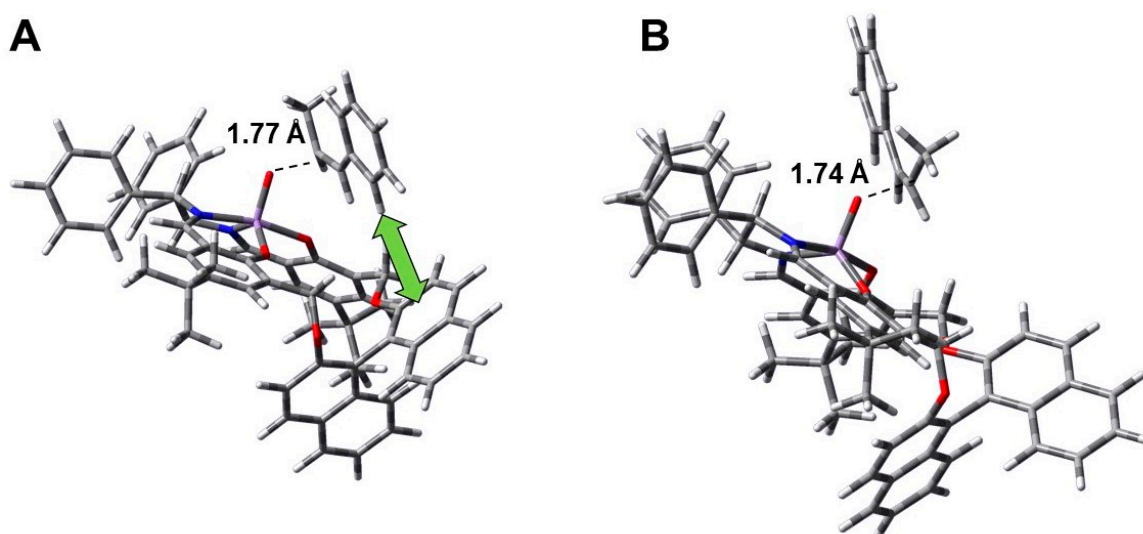


**Figure 4.** Three-dimensional plots of the two enantiomeric transition states for the epoxidation of cis-β-methyl-styrene with Mn-M20 leading to the (2S,3R) (A) and the (2R,3S) (B) epoxides, respectively. The green arrow highlights the CH-π interaction between the alkene and the aromatic ring of the BINOL compound.

Calculations supported the enantiomeric excess experimental results. The calculated activation energies were comparable in the two cases with values of about 7 and 8 kcal/mol in vacuo for the transition states leading to the (2*S*,3*R*) epoxide and the (2*R*,3*S*) epoxide, respectively (Figure 4). Considering the free energy values, the reaction was slower due to energy barriers of about 21 and 22 kcal/mol for the transition states leading to the (2*S*,3*R*) epoxide and the (2*R*,3*S*) epoxide, respectively. Thus, the transition state related to the (2*S*,3*R*) epoxide was favored (1.18 kcal/mol), probably due to the  $\pi$ - $\pi$  stacking interactions between the aromatic ring of the alkene and the salicylaldehyde ring of the catalyst, as well as the CH- $\pi$  interaction with the BINOL compound (showed by green arrows in Figure 4A). If the alkene attacks the Mn=O with the opposite face (Figure 4B) leading to the (2*R*,3*S*) epoxide, these interactions cannot be found.

The ratio between the two enantiomers on the basis of the transition state energies was 78:22 with a theoretical enantiomeric excess of 56% in vacuo. Considering methanol as a solvent, the energy barriers resulted in 10.62 and 11.02 kcal/mol for the transition states related to the (2*S*,3*R*) and (2*R*,3*S*) epoxides, respectively, with a ratio between the two enantiomers of 66:34 and a theoretical EE value of 32%, which was in line with the experimental one (Table 1, entry 2).

Taking into account these results and considerations, substituents in the 3,3'-positions play a crucial role in the determination of the enantioselectivity values. Their fundamental importance is probably ascribed to the stabilizing/destabilizing effect of the transition state, as showed in Figures 2a and 4A.

### 3. Materials and Methods

GC analyses of the epoxidation reaction were performed with a GC-FID (Flame Ionization Detector) instrument. The EE values were estimated and calculated by using a proper chiral column DMePeBETACDX (25 m  $\times$  0.25 mm ID  $\times$  0.25  $\mu$ m film) for 1,2-dihydronaphthalene (isotherm 150  $^{\circ}$ C) and DMeTButiSiliBETA (25 m  $\times$  0.25 mm ID  $\times$  0.25  $\mu$ m film) for *cis*- $\beta$ -methyl-styrene (column conditions: 50  $^{\circ}$ C (0 min) to 120  $^{\circ}$ C (1 min) at 2  $^{\circ}$ C/min). The injector and detector temperatures were maintained at 250  $^{\circ}$ C for both columns. As an internal standard, *n*-decane was used throughout. ESI mass spectra were obtained by employing an ES-MS equipped with an ion trap analyzer. The absolute configurations of (1*R*,2*S*)-1,2-epoxy-1,2,3,4-tetrahydronaphthalene and of (1*R*,2*S*)-1,2-epoxy-1-phenylpropane were determined by measuring the optical rotations with a polarimeter. Commercial reagents were used as received without further purification. All the calculations were performed using the Gaussian 16 program package [27]. Optimizations were done in the gas phase at the b3lyp/6-31g(d) level [28,29] for all atoms, while the b3lyp/def2svp was used for Mn to correctly describe the electronic properties of the systems. The solvent effects (CH<sub>3</sub>OH) were considered by single-point calculations at the same level as above using the self-consistent reaction field (SCRF) method based on the polarizable continuum solvent model (PCM) [30–32]. Vibrational frequencies were computed at the same level of theory to verify that the optimized structures were minimal. Thermodynamics at 298.15 K allowed the Gibbs free energies to be calculated.

#### 3.1. Synthesis of Mn Macrocyclic Catalysts

The absolute ethanol solution of the given macrocyclic salen-ligand was stirred overnight at room temperature with 1.5 equivalents of manganese(III) acetate in the case of M20 or with three equivalents of manganese(III) acetate in the case of M40. When the starting ligand was completely converted (checked by thin layer chromatography TLC analysis), the solvent was removed under reduced pressure. Then, 5 mL CH<sub>2</sub>Cl<sub>2</sub> was added to the remaining crude solid to dissolve the Mn complex. The residual precipitate (not reacted manganese (III) acetate) was removed and the CH<sub>2</sub>Cl<sub>2</sub> solution was concentrated in vacuo thus giving the corresponding catalyst with nearly quantitative yield.

Mn-M20: ESI-MS: detected  $m/z$ , 895  $[M]^+$  (expected, 895.3); analytically calculated values for  $C_{58}H_{52}MnN_2O_4$ : C, 77.75; H, 5.85; Mn, 6.13; N, 3.13; O, 7.14; values as measured: C, 77.71; Mn, 6.09; N, 3.10; O, 7.11.

Mn-M40-DiPh: ESI-MS: detected  $m/z$ , 895  $[M]^{2+}$  (expected, 895.8); analytically calculated values for  $C_{116}H_{104}Mn_2N_4O_8$ : C, 77.75; H, 5.85; Mn, 6.13; N, 3.13; O, 7.14; values as measured: C, 77.68; Mn, 6.07; N, 3.12; O, 7.10.

Mn-M40-Cycl: ESI-MS: detected  $m/z$ , 797  $[M]^{2+}$  (expected, 797.8); analytically calculated values for  $C_{100}H_{100}Mn_2N_4O_8$ : C, 75.27; H, 6.32; Mn, 6.89; N, 3.51; O, 8.02; values as measured: C, 75.17; Mn, 6.82; N, 3.48; O, 7.98.

### 3.2. General Procedure for Epoxidation Reactions

A dichloromethane solution of the substrate (0.35 mmol), chiral macrocycle catalyst (5%) and 4-phenylpyridine N-oxide (4-PPNO, 50%), buffered at pH 11.2 with a phosphate buffer, was stirred at 25 °C with bleach. The reaction was monitored using GC analysis by using *n*-decane as an internal quantitative standard. When the starting material was consumed, the organic phase was removed, dried with  $Na_2SO_4$  and purified by preparative layer chromatography (PLC) ( $SiO_2$ , cyclohexane/EtOAc (15:1, *v/v*). Absolute configurations were compared with literature data [33,34].

### 3.3. Computational Methods

Optimizations were done in the gas phase at the b3lyp/6-31g(d) level [28,29] for all atoms, while the b3lyp/def2svp was used for Mn to correctly describe the electronic properties of the systems. The solvent effects ( $CH_3OH$ ) were considered by single-point calculations at the same level as above using the self-consistent reaction field (SCRF) method based on the polarizable continuum solvent model (PCM) [30–32]. Vibrational frequencies were computed at the same level of theory to verify that the optimized structures were minimal. Thermodynamics at 298.15 K allowed the Gibbs free energies to be calculated. The  $\Delta E$  values and the percentages of the TS were calculated applying the Boltzmann equation. Using the obtained percentages, the EE values were calculated using the following equation:  $EE\% = [\% \text{ major compound} - \% \text{ minor compound}] / [\% \text{ major compound} + \% \text{ minor compound}] \times 100$ .

## 4. Conclusions

Three new chiral Mn macrocycle catalysts containing 20 or 40 atoms in the macrocycle were synthesized and tested in the enantioselective epoxidation of *cis*- $\beta$ -ethyl-styrene and 1,2-dihydronaphthalene. Reaction rates depend on the nature of the alkene and the presence of a coligand (PPNO) increases reaction rates, conversions and enantiomeric excesses. Despite the presence of a BINOL compound in the 3,3' position of the catalyst scaffolds, the enantioselectivities observed were, in general, low, probably due to the distance of these substituent with respect to the metal center. DFT calculations support this hypothesis. In particular, the calculated activation energies of the transition states related to the formation of the enantiomeric epoxides confirm the enantiomeric excesses obtained by experimental measurements.

**Supplementary Materials:** The following are available online at <https://www.mdpi.com/article/10.3390/catal11040465/s1>.

**Author Contributions:** Conceptualization, F.P.B. and G.T.S.; syntheses and epoxidation reactions, A.P. and R.M.T.; writing—original draft preparation, G.T.S.; conceived, designed, and supervised the computational study, M.A.C. and L.L.; performed the computational simulations and analyzed the in silico data, G.G. and L.V. All authors have read and agreed to the published version of the manuscript.

**Funding:** The authors thank the University of Catania for the financial support.

**Conflicts of Interest:** The authors declare no conflict of interest.

## References

1. Mc Garrigle, E.M.; Gilheany, D.G. Chromium- and Manganese-salen Promoted Epoxidation of Alkenes. *Chem. Rev.* **2005**, *105*, 1563–1602. [[CrossRef](#)] [[PubMed](#)]
2. Jacobsen, E.N.; Zhang, W.; Guler, M.L. Electronic tuning of asymmetric catalysts. *J. Am. Chem. Soc.* **1991**, *113*, 6703–6704. [[CrossRef](#)]
3. Katsuki, T. Catalytic asymmetric oxidations using optically active (salen) manganese(III) complexes as catalysts. *Coord. Chem. Rev.* **1995**, *140*, 189–214. [[CrossRef](#)]
4. Houk, K.N.; De Mello, N.C.; Condroski, K.; Fennen, J.; Kasuga, T. Origins of enantioselection in Jacobsen epoxidations. In Proceedings of the Electronic Conference on Heterocyclic Chemistry (ECHET96), London, UK, 24 June–22 July 1996.
5. La Paglia Fragola, V.; Lupo, F.; Pappalardo, A.; Trusso Sfrazzetto, G.; Toscano, R.M.; Ballistreri, F.P.; Tomaselli, G.A.; Gulino, A. A surface-confined O=Mn<sup>V</sup>(salen) oxene catalyst and high turnover values in asymmetric epoxidation of unfunctionalized olefins. *J. Mat. Chem.* **2012**, *22*, 20561. [[CrossRef](#)]
6. Hosoya, N.; Hatayama, A.; Yanai, K.; Fujii, H.; Irie, R.; Katsuki, T. Asymmetric epoxidation with optically active (salen) manganese(III) complexes: From which direction does the olefin approach the metal-oxo bond? *Synlett* **1993**, *9*, 641–645. [[CrossRef](#)]
7. Hamada, T.; Irie, R.; Katsuki, T. How does chiral oxo(salen) manganese(V) complex discriminate the enantioface of simple olefins? Scope and limitation of salen-catalyzed epoxidation. *Synlett* **1994**, *7*, 479–481. [[CrossRef](#)]
8. Jacobsen, E.N.; Zhang, W.; Muci, A.R.; Ecker, J.R.; Deng, L. Highly enantioselective epoxidation catalysts derived from 1,2-diaminocyclohexane. *J. Am. Chem. Soc.* **1991**, *113*, 7063–7064. [[CrossRef](#)]
9. Pospisil, P.J.; Carsten, D.H.; Jacobsen, E.N. X-ray structural studies of highly enantioselective Mn(salen) epoxidation catalysts. *Chem. A Eur. J.* **1996**, *2*, 974–980. [[CrossRef](#)]
10. Hashihayata, T.; Punniyamurthy, T.; Irie, R.; Katsuki, T.; Akita, M.; Moro-oka, Y. Conformational analysis of cationic (R, S)- and (R, R)-(salen) manganese complexes possessing axial chirality as a chiral element based on x-ray crystallography: An explanation of the effect of apical ligand on enantioselection by (salen) manganese catalyst. *Tetrahedron* **1999**, *55*, 14599–14610.
11. Katsuki, T. Chiral metallosalen complexes: Structures and catalyst tuning for asymmetric epoxidation and cyclopropanation. *Adv. Synth. Catal.* **2002**, *344*, 131–147. [[CrossRef](#)]
12. Zhang, W.; Loebach, J.L.; Wilson, S.R.; Jacobsen, E.N. Enantioselective epoxidation of unfunctionalized olefins catalyzed by salen manganese complexes. *J. Am. Chem. Soc.* **1990**, *112*, 2801–2803. [[CrossRef](#)]
13. Jacobsen, H.; Cavallo, L. A possible mechanism for enantioselectivity in the chiral epoxidation of olefins with [Mn(salen)] catalysts. *Chem. A Eur. J.* **2001**, *7*, 800–807. [[CrossRef](#)]
14. Kurti, L.; Blewett, M.M.; Corey, E.J. Origin of Enantioselectivity in the Jacobsen Epoxidation of Olefins. *Org. Lett.* **2009**, *11*, 4592–4595. [[CrossRef](#)]
15. Brown, M.K.; Blewett, M.M.; Colombe, J.R.; Corey, E.J. Mechanism of the Enantioselective Oxidation of Racemic Secondary Alcohols Catalyzed by Chiral Mn(III)-Salen Complexes. *J. Am. Chem. Soc.* **2010**, *132*, 11165–11170. [[CrossRef](#)]
16. Amato, M.E.; Ballistreri, F.P.; Pappalardo, A.; Sciotto, D.; Tomaselli, G.A.; Toscano, R.M. Synthesis and conformational aspects of 20- and 40-membered macrocyclic mono and dinuclear uranyl complexes incorporating salen and (R)-BINOL units. *Tetrahedron* **2007**, *63*, 9751–9757. [[CrossRef](#)]
17. Amato, M.E.; Ballistreri, F.P.; Gentile, S.; Pappalardo, A.; Tomaselli, G.A.; Toscano, R.M. Recognition of Achiral and Chiral Ammonium Salts by Neutral Ditopic Receptors Based on Chiral Salen-UO<sub>2</sub> Macrocycles. *J. Org. Chem.* **2010**, *75*, 1437–1443. [[CrossRef](#)]
18. Patti, A.; Pedotti, S.; Ballistreri, F.P.; Trusso Sfrazzetto, G. Synthesis and Characterization of Some Chiral Metal-Salen Complexes Bearing a Ferrocenophane Substituent. *Molecules* **2009**, *14*, 4312–4325. [[CrossRef](#)] [[PubMed](#)]
19. Trusso Sfrazzetto, G.; Millesi, S.; Pappalardo, A.; Toscano, R.M.; Ballistreri, F.P.; Tomaselli, G.A.; Gulino, A. Olefin epoxidation by a (salen)Mn(III) catalyst covalently grafted on glass beads. *Catal. Sci. Technol.* **2015**, *5*, 673–679. [[CrossRef](#)]
20. Ballistreri, F.P.; Toscano, R.M.; Amato, M.E.; Pappalardo, A.; Gangemi, C.M.A.; Spidalieri, S.; Puglisi, R.; Trusso Sfrazzetto, G. A New Mn-Salen Micellar Nanoreactor for Enantioselective Epoxidation of Alkenes in Water. *Catalysts* **2018**, *8*, 129. [[CrossRef](#)]
21. Zammataro, A.; Gangemi, C.M.A.; Pappalardo, A.; Toscano, R.M.; Puglisi, R.; Nicotra, G.; Fragalà, M.E.; Tuccitto, N.; Trusso Sfrazzetto, G. Covalently functionalized carbon nanoparticles with a chiral Mn-Salen: A new nanocatalyst for enantioselective epoxidation of alkenes. *Chem. Commun.* **2019**, *55*, 5255–5258. [[CrossRef](#)]
22. Ballistreri, F.P.; Gangemi, M.A.; Pappalardo, A.; Tomaselli, G.A.; Toscano, R.M.; Trusso Sfrazzetto, G. (Salen)Mn(III) Catalyzed Asymmetric Epoxidation Reactions by Hydrogen Peroxide in Water: A Green Protocol. *Int. J. Mol. Sci.* **2016**, *17*, 1112. [[CrossRef](#)]
23. Legnani, L.; Iannazzo, D.; Pistone, A.; Celesti, C.; Giofrè, S.; Romeo, R.; Di Pietro, A.; Visalli, G.; Fresta, M.; Bottino, P.; et al. Functionalized polyhedral oligosilsesquioxane (POSS) based composites for bone tissue engineering: Synthesis, computational and biological studies. *RSC Adv.* **2020**, *10*, 11325–11334. [[CrossRef](#)]
24. Legnani, L.; Puglisi, R.; Pappalardo, A.; Chiacchio, M.A.; Trusso Sfrazzetto, G. Supramolecular recognition of phosphocholine by an enzyme-like cavitand receptor. *Chem. Commun.* **2020**, *56*, 539–542.
25. Chiacchio, M.A.; Legnani, L.; Caramella, P.; Tejero, T.; Merino, P. Revealing carbocations in highly asynchronous concerted reactions: The ene-type reaction between dithiocarboxylic acids and alkenes. *Tetrahedron* **2018**, *74*, 5627–5634. [[CrossRef](#)]

26. Chiacchio, M.A.; Legnani, L.; Caramella, P.; Tejero, T.; Merino, P. Pivotal Neighboring-Group Participation in Substitution versus Elimination Reactions—Computational Evidence for Ion Pairs in the Thionation of Alcohols with Lawesson’s Reagent. *Eur. J. Org. Chem.* **2017**, *14*, 1952–1960. [[CrossRef](#)]
27. Frisch, M.J.; Trucks, G.W.; Schlegel, H.B.; Scuseria, G.E.; Robb, M.A.; Cheeseman, J.R.; Scalmani, G.; Barone, V.; Petersson, G.A.; Nakatsuji, H.; et al. *Gaussian 16, Revision C.01*; Gaussian, Inc.: Wallingford, CT, USA, 2016.
28. Becke, A.D. Density-functional thermochemistry. III. The role of exact exchange. *J. Chem. Phys.* **1993**, *98*, 5648–5652. [[CrossRef](#)]
29. Lee, C.; Yang, W.; Parr, R.G. Development of the Colle-Salvetti correlation-energy formula into a functional of the electron density. *Phys. Rev. B* **1988**, *37*, 785–789. [[CrossRef](#)] [[PubMed](#)]
30. Cancès, E.; Mennucci, B.; Tomasi, J. A new integral equation formalism for the polarizable continuum model: Theoretical background and applications to isotropic and anisotropic dielectrics. *J. Chem. Phys.* **1997**, *107*, 3032–3042. [[CrossRef](#)]
31. Cossi, M.; Barone, V.; Cammi, R.; Tomasi, J. Ab initio study of solvated molecules: A new implementation of the polarizable continuum model. *Chem. Phys. Lett.* **1996**, *255*, 327–335. [[CrossRef](#)]
32. Barone, V.; Cossi, M.; Tomasi, J. Geometry optimization of molecular structures in solution by the polarizable continuum model. *J. Comput. Chem.* **1998**, *19*, 404–417. [[CrossRef](#)]
33. Sasaki, H.; Irie, R.; Hamada, T.; Suzuki, K.; Katsuki, T. Rational design of Mn-salen catalyst. 2: Highly enantioselective epoxidation of conjugated cis-olefins. *Tetrahedron* **1994**, *50*, 11827–11838. [[CrossRef](#)]
34. Irie, R.; Noda, K.; Ito, Y.; Matsumoto, N.; Katsuki, T. Catalytic asymmetric epoxidation of unfunctionalized olefins using chiral (salen) manganese(III) complexes. *Tetrahedron Asymmetry* **1991**, *2*, 481–494. [[CrossRef](#)]